Bioorganic & Medicinal Chemistry 18 (2010) 496–507

Contents lists available at ScienceDirect

Bioorganic & Medicinal Chemistry

journal homepage: www.elsevier.com/locate/bmc

Design and pharmacophore modeling of biaryl methyl eugenol analogs as breast cancer invasion inhibitors

Fatma M. Abdel Bar [†,‡], Mohammad A. Khanfar [†], Ahmed Y. Elnagar [†], Farid A. Badria [‡], Ahmed M. Zaghloul [‡], Kadria F. Ahmad [‡], Paul W. Sylvester [†], Khalid A. El Sayed [*,†]

Department of Basic Pharmaceutical Sciences, College of Pharmacy, University of Louisiana at Monroe, 700 University Avenue, Monroe, LA 71209, USA
Department of Pharmacognosy, Faculty of Pharmacy, Mansoura University, Mansoura 35516, Egypt

ARTICLE INFO

Article history:
Received 6 October 2009
Revised 3 December 2009
Accepted 5 December 2009
Available online 11 December 2009

Keywords:
Anti-invasive
Biaryl
Breast cancer
Heck and Suzuki coupling reactions
Methyl eugenol
Microtubules
Pharmacophore modeling

ABSTRACT

Cell invasion and migration are required for the parent solid tumor cells to metastasize to distant organs. Microtubules form a polarized network, enabling organelle and protein movement throughout the cell. Cytoskeletal elements coordinately regulate cell's motility, adhesion, migration, exocytosis, endocytosis, and division. Thus, microtubule disruption can be a useful target to control cancer cell invasion and metastasis. The phenolic ether methyl eugenol (**1**), the major component of the essential oil of the leaves of *Melaleuca ericifolia* Sm. (Myrtaceae), was used as a starting scaffold to design eleven new and three known anti-tubulin agents **2**–**15** using carbon–carbon coupling reactions. A computer-assisted approach was used to design these new biaryl derivatives using colchicine-binding site of tubulin as the molecular target and colchicine as an active ligand. Several derivatives showed potent inhibitory activity against MDA-MB-231 cell migration at the 1–4 μM dose range. The *Z* isomers, **4** and **15** were more active as invasion inhibitors compared to their structurally related *E* isomers, **2** and **14**. The cytotoxic activities of compounds **2**–**15** against two breast cancer cell lines MDA-MB-231 and MCF-7 were evaluated. Anti-invasive activity of the semisynthetic derivatives is not due to a direct cytotoxic effect on MDA-MB-231. Analogs **2**–**15** may promote their anti-invasive activity through the induction of changes in cell morphology. A pharmacophore model was generated involving seven essential features for activity, which was consistent with a previously generated colchicine site inhibitors model.

1. Introduction

Breast cancer is the most common cancer representing nearly 25% of total diagnosed cancer cases and the second leading cause of female cancer deaths in America.[1] Metastasis rather than the primary tumor kills 90% of cancer patients. Patient progression at the metastatic stage of disease is very poor, and currently there are few available treatment options.[1] Controlling the invasion and metastasis of primary tumor cells and preventing their spread to distant and vital organs are major challenges in cancer therapy.

The cytoskeleton is composed of actin, microtubule, and intermediate microfilaments.[1,2] Cytoskeleton proteins constitute over 25% of total proteins in the cell.[1–3] Cytoskeleton proteins play an important role in invasion and metastasis of tumor cells.[1,2] Microtubules play a critical role in formation of the mitotic spindle, which provides the structural framework for the physical segregation of chromosomes during cell division (mitosis).[5–7] The formation of microtubules is a dynamic process that involves the assembly of heterodimers formed by α- and β-tubulin subunits and degradation or disassembly of the linear polymers.[3–7] The normal function of tubulin assembly and disassembly is thus crucial for cell division, and any interference with this process will disrupt cell division and induce cell death by apoptosis.[3–7] Microtubule dynamics are implicated in many cellular processes including adhesion, migration, and morphology.[5–7] Thus, tubulin inhibitors can impair the invasiveness potential of cancer cells.[5–7]

Tubulin polymerization inhibitors, for example, vinca alkaloids, combretastatins and colchicine and tubulin polymerization promoters, for example, taxanes like paclitaxel, are examples of anticancer tubulin/microtubule-targeting drugs.[6,7] The importance of microtubules as molecular targets has been amplified by the discovery of potent and selective toxicity of combretastatin A4 (CA4) as a vascular-disrupting agent (VDA).[2,3] Vascular-disrupting agents (VDAs) selectively impair tumor's vasculature which is essential for tumor progression and metastasis. The water-soluble prodrug of CA4, combretastatin-A4 phosphate (CA4P), is currently in phase II clinical trials.[4] Paclitaxel is unique in its mechanism, promoting the assembly of tubulin into highly stable non-functional polymers.[6,7] The mechanism by which paclitaxel stabilizes

* Corresponding author. Tel.: +1 318 342 1725; fax: +1 318 342 1737.
E-mail address: elsayed@ulm.edu (K.A. El Sayed).
† University of Louisiana at Monroe, USA.
‡ Mansoura University, Egypt.

0968-0896/$ - see front matter © 2009 Elsevier Ltd. All rights reserved.
doi:10.1016/j.bmc.2009.12.019

the microtubules is still under investigation.[6] So far, three binding domains have been identified in the crystal structure of tubulin; (i) the cholchicine site, which is close to the α/β interface, (ii) the area where vinca alkaloids bind, and (iii) the taxane binding pocket.[7]

Methyl eugenol (**1**, 4-allyl-1,2-dimethoxybenzene) is a widely distributed naturally occurring phenolic ether in a variety of plant species. It represents 96.8% of the content of the volatile oil of *Melaleuca ericifolia* Sm. grown in Egypt.[8] This study reports a series of rationally designed tubulin-targeting biaryl derivatives (**2**–**15**), which were prepared semisynthetically starting with **1** using Heck and Suzuki coupling reactions. Their structure design was based on molecular docking studies in SYBYL 8.1 and close structure similarity to chalcones, the biaryl enones that showed potent toxicity to several cancer cell lines and interact with tubulin at its colchicine-binding site.[7]

The new biaryl compounds have been tested for ability to inhibit cell invasion in the MDA-MB-231 breast cancer cell line. The cytotoxicity of **2**-**15** against the MDA-MB-231 and MCF-7 breast cancer cell lines has also been studied.

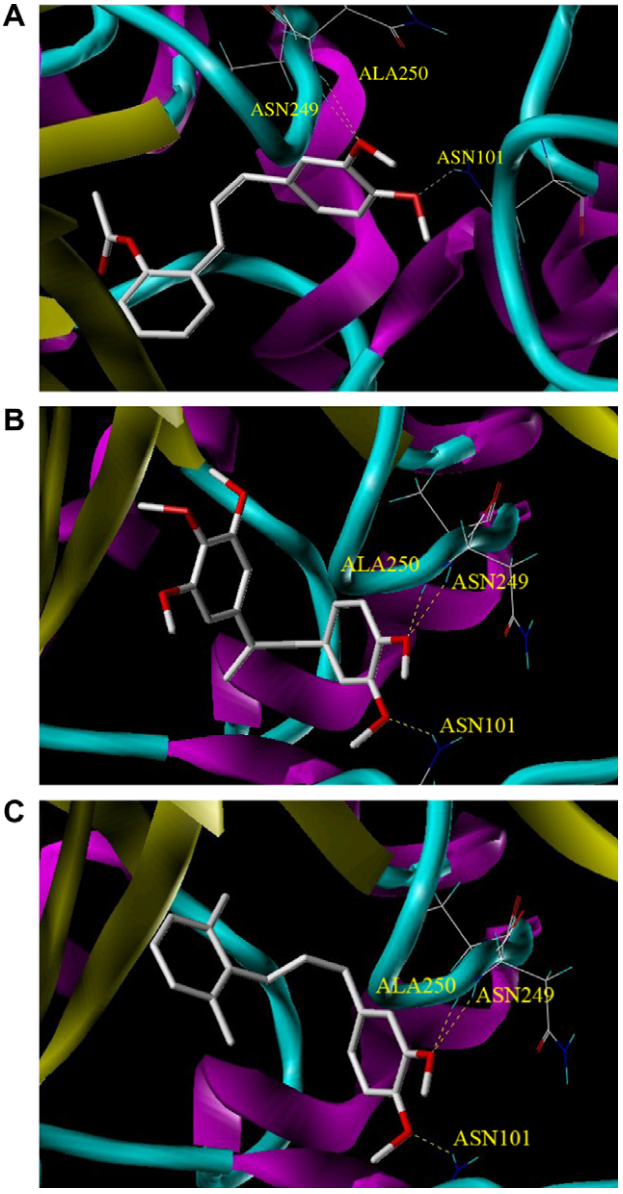

Figure 1. Detailed view of docked structures **4** (A), **9** (B), and **14** (C) with the corresponding interacting amino acids of tubulin binding site.

2. Results and discussion

2.1. Molecular modeling and docking study

Grams of methyl eugenol **1** were isolated from the volatile oil of *M. ericifolia* Sm. grown in Egypt.[8] To design a series of coupling products of **1** with diverse aryl moieties, a computer-aided molecular modeling study was carried out within the colchicine-binding site of the high-resolution crystal structure (resolution = 3.80 Å) of the tubulin–colchicine–soblidotin: stathmin-like domain complex (PDB 3e22).[9] The protein crystal structure was retrieved from the Research Collaboratory for Structural Bioinformatics Protein Data Bank. The structure of colchicine was used as a reference ligand along the docking and modeling studies.

In silico docking indicated two interactions with β-tubulin (alanine 250, ALA 250) and asparagine 250, ASN 249) and one with α-tubulin (asparagine 101, ASN 101) via strong H-bonding with the 3,4-dimethoxy functionality in the methyl eugenol moiety (Fig. 1). These results were consistent with the fact that colchicine-binding site is deeply buried within the β-tubulin.[10,11] The binding modes of the designed structures were found to be comparable to the interaction maps of other anti-tubulin agents.[12]

Several biaryl carbon–carbon coupling structures of **1** with 2-acetoxy, 2-methoxy, 4-methoxy, and 3,4,5-trimethoxyphenyl functionalities showed improved binding affinities at the colchicine-binding site as suggested by the high total scores of **2–4**, **6**, **9**, and **11–14**, compared to colchicine (Table 1). To test whether electron-donating alkyl groups like methyl will show improved activity versus methoxy groups, compounds **14** and **15** were proposed.[13] Thus, compounds **2**–**15** were synthesized and tested for their cytotoxic and anti-invasive activities.

2.2. Chemical synthesis

Compounds **2**–**4**, **14**, and **15** were prepared by using Heck's coupling reaction between the alkene group of methyl eugenol (**1**) and aryl halides (Scheme 1).[14] Compounds **5**–**13** were prepared using oxygen-promoted Pd(II) catalysis for the coupling of aryl boronic acids and the $\Delta^{2,3}$ alkene system of **1** (Suzuki coupling, Scheme 2).[15] Both *E* and *Z* isomers have been observed as products in the Heck reaction with the *E*-adduct more predominant than the *Z*-adduct, which was a minor product (Scheme 1). Suzuki coupling was

Table 1
Virtual binding affinity of compounds **2**–**15** at the colchicine-binding site of tubulin (PDB 3e22) using SYBYL 8.1 Surflex-Dock[a]

Compound	Total	Crash	Polar	C Score
3	8.51	−1.64	2.64	4
6	8.40	−1.93	2.90	2
12	8.28	−1.51	1.73	2
9	8.25	−3.22	2.78	4
2	7.97	−2.79	2.64	2
4	7.97	−2.16	1.06	5
13	7.81	−2.66	0.57	2
11	7.57	−1.61	0.00	4
14	7.53	−2.92	2.65	2
Colchicine	7.52	−1.50	1.01	5
10	7.45	−1.79	1.20	4
7	7.03	−1.22	0.00	2
5	6.92	−3.74	1.39	4
8	6.92	−3.74	1.39	2
15	6.19	−1.08	0.00	2

[a] Total score was expressed in $-\log(K_d)$ units to represent binding affinities. Crash is the degree of inappropriate penetration by the ligand into the protein and of interpenetration between ligand atoms that are separated by rotatable bonds. Polar score is the contribution of the polar non-hydrogen bonding interactions to the total score. The polar score may be useful for excluding docking results that make no hydrogen bonds.

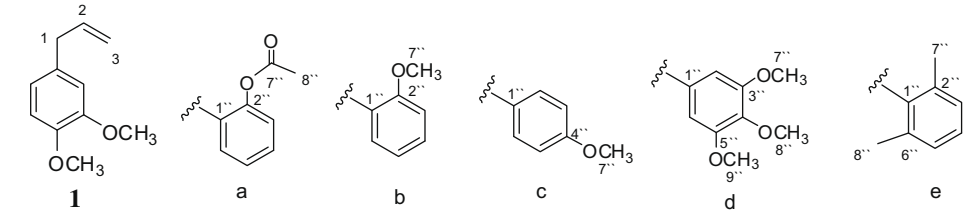

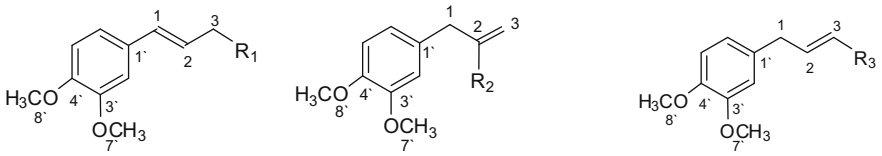

	R_1		R_2		R_3
2	a	**3**	a	**7**	c
5	b	**6**	c	**11**	d
8	c	**9**	d	**14**	e
10	d				

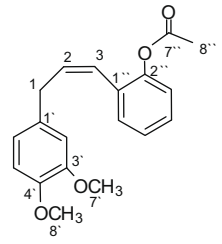

4

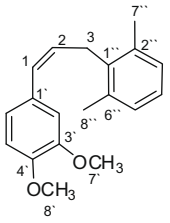

15

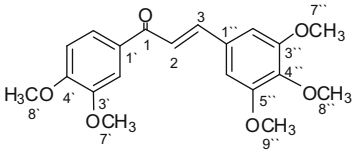

12

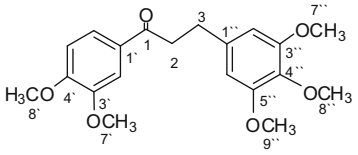

13

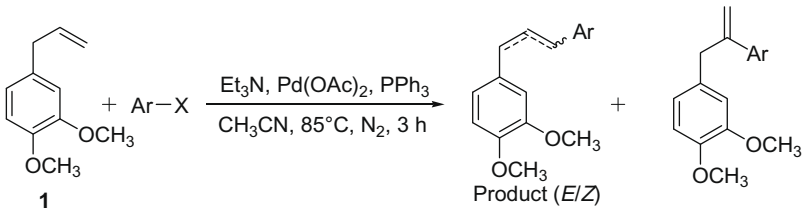

Scheme 1. Heck coupling reaction between methyl eugenol olefinic side chain and aryl halides used for the preparation of **2**–**4**, **14**, and **15**.

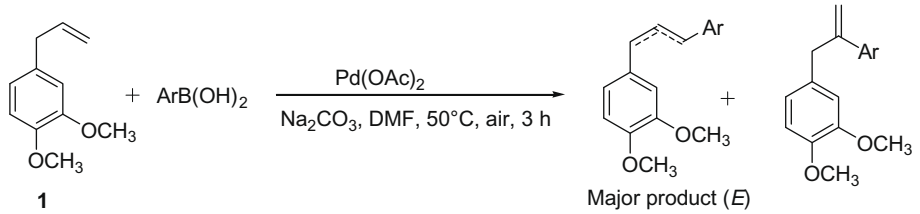

Scheme 2. Suzuki coupling reaction between methyl eugenol olefinic side chain and aryl boronic acids used for the preparation of **5**–**13**.

Table 2
^{1}H NMR data of compounds **2**–**4**, **6**, and **7**[a]

Position	δ_H				
	2	**3**	**4**	**6**	**7**
1	6.35, d (15.7)	3.60, s	3.48, d (5.5)	3.74, s	3.46, d (7.0)
2	6.09, dt (15.8, 6.6)	—	6.34, dt (7.7, 5.8)	—	6.15,dt (15.8, 7.0)
3	3.44, d (6.6)	5.07, d (1.5) 5.08, br s	6.36, d (7.7)	4.95, s 5.40, s	6.36, d (15.8)
1′	—	—	—	—	—
2′	6.88, d (1.8)	6.64, d (1.8)	6.73, d (2.2)	6.76, s	6.74, d (1.8)
3′	—	—	—	—	—
4′	—	—	—	—	—
5′	6.78, d (8.0)	6.75, d (8.0)	6.81, d (8.4)	6.74, d (8.1)	6.80, d (8.1)
6′	6.85, dd (8.0, 1.8)	6.67, dd (8.0, 1.8)	6.74, dd (8.0, 1.8)	6.74, d (8.1)	6.76, dd (8.1, 1.8)
7′	3.86, s	3.80, s	3.87, s	3.81, s	3.86, s
8′	3.87, s	3.84, s	3.86, s	3.83, s	3.86, s
1″	—	—	—	—	—
2″	—	—	—	7.35, d (8.4)	7.28, d (8.8)
3″	7.03, dd (7.7, 1.5)	7.01, d (8.0)	6.99, dd (7.7, 1.1)	6.80, d (8.1)	6.82, d (8.8)
4″	7.24, dd (7.7, 1.8)	7.23, dd (2.2, 8.4)	7.51, dd (7.7, 1.8)	—	—
5″	7.19, dd (7.3, 1.5)	7.11, dd (7.7, 1.1)	7.21, dd (7.7, 1.8)	6.80, d (8.1)	6.80, d (8.8)
6″	7.29, dd (7.3, 1.5)	7.09, dd (7.7, 2.2)	7.18, dd (7.4, 1.5)	7.35, d (8.4)	7.28, d (8.8)
7″	—	—	—	3.78, s	3.80, s
8″	2.28, s	2.26, s	2.26, s		

[a] In $CDCl_3$, at 400 MHz. Coupling constants (J) are in Hz.

selective to *E*-geometry only. The location of the $\Delta^{2,3}$ system adjacent to the aliphatic methylene carbon C-1 in **1** allowed its migration to the $\Delta^{1,2}$ position in some products during the coupling reaction. Additionally, coupling may occasionally target the olefinic methine carbon C-2 instead of the olefinic methylene carbon C-3 of **1**, resulting in the formation of minor C_6–C_2–C_6 products with an exomethylene group as in compounds **3**, **6**, and **9** along with the major C_6–C_3–C_6 products. Compounds **5**, **12**, and **13** are already known in literature.[16,17]

The HRESIMS data of **2** (m/z 335.1265 for $[M+Na]^+$) suggested the molecular formula $C_{19}H_{20}O_4$. ^{1}H NMR data of **2** (Table 2) showed a doublet at δ 6.35 (J = 15.7) assigned to H-1 and a double triplet at δ 6.09 (J = 15.8, 6.6) assigned to H-2 and indicated a possible *E*-geometry for $\Delta^{1,2}$ system and hence *trans*-coupling of the 2-acetoxyphenyl moiety with **1**. The ^{13}C NMR data of **2** (Table 3) showed 19 carbon signals, which further confirmed the identity of **2** as a carbon–carbon coupling product. The presence of the acetoxy methyl singlet H_3-8″ at δ 2.27 in addition to seven aromatic protons further supported this conclusion. The proton doublet H-1 showed ^3J-HMBC correlations with C-3, C-2′, and C-6′ (δ_C 33.9, 108.5, and 119.2, respectively). The proton H-2 showed ^3J-HMBC correlations with C-1′, and C-1″ (δ_C 130.5 and 132.2, respectively). The ^3J-HMBC correlation of the methylene proton doublet H_2-3 (δ_H 3.44) with carbons C-2″ and C-6″ (δ_C 148.5 and 127.6, respectively) indicated the migration of $\Delta^{2,3}$ of the parent **1** to $\Delta^{1,2}$ during the reaction. Therefore, the structure of **2** was determined to be (*E*)-2-[3-(3,4-dimethoxyphenyl)allyl]phenyl acetate.

Table 3
^{13}C NMR data of compounds **2**–**4**, **6**, and **7**[a]

Position	δ_C				
	2	**3**	**4**	**6**	**7**
1	132.2, CH	42.8, CH_2	39.3, CH_2	41.4, CH_2	39.0, CH_2
2	125.8, CH	145.8, qC	124.3, CH	146.4, qC	127.4, CH
3	33.9, CH_2	116.7, CH_2	132.3, CH	112.9, CH_2	130.3, CH
1′	130.5, qC	131.5, qC	132.3, qC	132.3, qC	133.1, qC
2′	108.5, CH	112.4, CH	111.9, CH	111.2, CH	112.0, CH
3′	149.1, qC	148.7, qC	149.0, qC	148.9, qC	149.0, qC
4′	149.0, qC	147.4, qC	147.8, qC	147.4, qC	147.5, qC
5′	111.1, CH	111.0, CH	111.2, CH	112.2, CH	111.4, CH
6′	119.2, CH	121.3, CH	120.7, CH	120.9, CH	120.6, CH
7′	56.0, CH_3	55.9, CH_3	55.9, CH_3	55.9, CH_3	55.9, CH_3
8′	55.9, CH_3	55.8, CH_3	56.0, CH_3	55.8, CH_3	56.0, CH_3
1″	132.2, qC	135.6, qC	130.1, qC	133.4, qC	130.6, qC
2″	148.5, qC	147.6, qC	147.5, qC	127.3, CH	127.3, CH
3″	122.6, CH	122.6, CH	122.6, CH	113.7, CH	114.0, CH
4″	130.7, CH	128.3, CH	126.8, CH	159.1, qC	159.0, qC
5″	126.4, CH	126.0, CH	128.1, CH	113.7, CH	114.0, CH
6″	127.6, CH	130.0, CH	126.3, CH	127.3, CH	127.3, CH
7″	169.6, qC	169.6, qC	169.5, qC	55.3, CH_3	55.4, CH_3
8″	21.1, CH_3	21.2, CH_3	20.97, CH_3		

[a] In $CDCl_3$, at 100 MHz. Carbon multiplicities were determined by APT experiment. qC = quaternary, CH = methine, CH_2 = methylene, CH_3 = methyl carbons.

Analysis of HRESIMS of **3** (m/z 335.1250 for $[M+Na]^+$) suggested the same molecular formula as **2** and indicated a coupling product. The ^{1}H NMR data of **3** (Table 2) showed a benzylic methylene singlet at δ 3.60, assigned to H_2-1 and exomethylene protons H-3a and H-3b (δ_H 5.07 and 5.08, respectively). This indicated a possible coupling product at C-2 rather than the expected C-3 of the parent compound **1**. The ^{13}C NMR data of **3** (Table 3) showed a $\Delta^{2,3}$ typical exomethylene pattern with a quaternary carbon at δ 145.8 (C-2) and olefinic exomethylene at δ 116.7 (C-3). The exomethylene protons H-3a and H-3b showed ^3J-HMBC correlations of with the methylene carbon C-1 (δ_C 42.8) and the quaternary aromatic C-1″ (δ_C 135.6). It also showed a ^2J-HMBC correlation with C-2, confirming the coupling at C-2 of the side chain of **1**. Therefore, compound **3** was determined to be 2-[3-(3,4-dimethoxyphenyl)prop-1-en-2-yl]phenyl acetate.

The HRESIMS data of **4** (m/z 335.1257 for $[M+Na]^+$) suggested it is an isomer of **2** and **3**. The ^{1}H NMR data of **4** (Table 2) showed two overlapped protons H-2 and H-3 (δ_H 6.34, J = 7.7, 5.8 and 6.36, J = 7.7, respectively). Their coupling constant values indicated the *Z*-geometry for $\Delta^{2,3}$ system and hence *cis*-coupling of the 2-acetoxyphenyl moiety with **1**. The methylene protons H_2-1 (δ_H 3.48) showed ^3J-HMBC correlations with C-3, C-2′, and C-6′ (δ_C 132.3, 111.9, and 120.7, respectively), in addition to ^2J-HMBC correlation with the quaternary carbon C-1′ (δ_C 132.3), indicated an expected carbon–carbon coupling pattern at C-3 of **1**. Therefore, compound **4** was determined to be (*Z*)-2-[3-(3,4-dimethoxyphenyl)prop-1-enyl]phenyl acetate.

Analysis of the HRESIMS data of **6** (m/z 307.1310 for $[M+Na]^+$) suggested the molecular formula $C_{18}H_{20}O_3$ and indicated a coupling product of **1** with 4-methoxyphenyl moiety. The ^{1}H and ^{13}C NMR spectrum of **6** (Tables 2 and 3, respectively) suggested a coupling product similar to **3**. The methoxy proton singlet H_3-7″ (δ_H 3.78)

Table 4
^{1}H NMR data of compounds **8**–**11** and **14**–**15**[a]

Position	δ_H					
	8	**9**	**10**	**11**	**14**	**15**
1	6.34, d (15.7)	3.73, s	6.37, d (15.8)	3.47,d (5.9)	3.52, d (7.0)	3.53, d (4.4)
2	6.16, dt (15.7, 7.0)	—	6.15, dt (15.4, 7.0)	6.21, dt (15.4, 6.6)	5.77, dt (16.1, 7.0)	6.13, dt (5.5, 4.4)
3	3.46, d (7.0)	5.00, s 5.41, s	3.46, d (7.0)	6.33, d (15.8)	6.39, d (16.1)	6.14, d (5.5)
1′	—	—	—	—	—	—
2′	6.90, d (1.8)	6.78, br s	6.92, d (1.8)	6.75, d (1.8)	6.81, d (2.6)	6.85, d (1.8)
3′	—	—	—	—	—	—
4′	—	—	—	—	—	—
5′	6.78, d (8.4)	6.75, br d (10.6)	6.79, d (8.1)	6.82, d (8.0)	6.81, d (2.6)	6.76, d (8.0)
6′	6.86, dd (8.1, 1.8)	6.75, br d (10.6)	6.89, dd (8.1, 1.8)	6.79, d (8.0, 1.8)	6.81, d (2.6)	6.81, d (8.0, 1.8)
7′	3.86, s	3.84, s	3.87, s	3.87, s	3.87, s	3.85, s
8′	3.87, s	3.82, s	3.88, s	3.87, s	3.87, s	3.86, s
1″	—	—	—	—	—	—
2″	7.15, d (8.8)	6.62, s	6.45, s	6.58, s	—	—
3″	6.85, d (8.8)	—	—	—	7.02, m	7.02, d (1.8)
4″	—	—	—	—	7.02, m	7.02, d (1.8)
5″	6.85, d (8.8)	—	—	—	7.02, m	7.02, d (1.8)
6″	7.15, d (8.8)	6.62, s	6.45, s	6.58, s	—	—
7″	3.79, s	3.81, s	3.85, s	3.85, s	2.30, s	2.34, s
8″		3.82, s	3.83, s	3.83, s	2.30, s	2.34, s
9″		3.81, s	3.85, s	3.85, s		

[a] In $CDCl_3$, at 400 MHz. Coupling constants (*J*) are in Hz.

showed a ^3J-HMBC correlation with the quaternary aromatic oxygenated carbon C-4″ (δ_C 159.1). The aromatic proton doublet H-2″ (δ_H 7.35) showed ^3J-HMBC-correlations with the quaternary olefinic carbons C-2 (δ_C 146.4) and C-4″. Therefore, the structure of **6** was determined to be 1,2-dimethoxy-4-[2-(4-methoxyphenyl)allyl] benzene.

The HRESIMS data of **7** (*m*/*z* 307.1313 for $[M+Na]^+$) suggested a similar molecular formula as **6**. The ^{1}H and ^{13}C NMR data of **7** (Tables 2 and 3, respectively) indicated an expected coupling product at C-3 of **1**. The large coupling value between H-2 (δ_H 6.15, *J* = 15.8, 7.0) and H-3 (δ_H 6.36, *J* = 15.8) indicated a possible *E*-geometry for $\Delta^{2,3}$ system and hence the *trans*-coupling of the 3,4,5,-trimethoxyphenyl moiety with C-3 of **1**. The methylene H_2-1 (δ_H 3.46) showed ^3J-HMBC correlations with carbons C-3, C-2′, and C-6′ (δ_C 130.3, 112.0, and 120.6, respectively). It also showed a ^2J-HMBC correlation with the quaternary carbon signal at δ 133.1 (C-1′) indicated a similar pattern of the double bond position to **1**. Therefore, the structure of **7** was determined to be (*E*)-1,2-dimethoxy-4-[3-(4-methoxyphenyl)allyl]benzene.

The HREIMS data of **8** (*m*/*z* 307.1313 for $[M+Na]^+$) has the same molecular formula and was very closely similar to **7**. The ^{1}H and ^{13}C NMR data of **8** (Tables 4 and 5, respectively) revealed a *trans*-coupling product closely similar to **2**, with the replacement of 2-acetoxyphenyl with a 4-methoxyphenyl moiety. ^{13}C NMR data of **8** show some differences in chemical shift values were clearly observed than in case of **7**. The symmetric aromatic carbons C-2″/C-6″ were downfield shifted (+2.4 ppm) while C-2′ and C-6′ were upfield shifted (−3.5 and −1.4 ppm, respectively) compared to those of **7**. These chemical shift differences were mainly due to the migration of $\Delta^{2,3}$ of **1** to $\Delta^{1,2}$ during the coupling reaction similar to **2** and **5**. Therefore, the structure of **8** was determined to be (*E*)-1,2-dimethoxy-4-[3-(4-methoxyphenyl)prop-1-enyl]benzene.

The HRESIM of **9** (*m*/*z* 367.1509 for $[M+Na]^+$) suggested the molecular formula $C_{20}H_{24}O_5$, suggesting a coupling product of **1**

Table 5
^{13g}C NMR data of compounds **8**–**11** and **14**–**15**[a]

Position	δ_C					
	8	**9**	**10**	**11**	**14**	**15**
1	130.4, CH	41.4, CH_2	130.8, qC	38.9, CH_2	39.5, CH_2	129.8, CH
2	127.9, CH	147.3, qC	127.2, CH	129.1, CH	134.3, CH	126.2, CH
3	38.5, CH_2	114.2, CH_2	39.8, CH_2	130.8, CH	128.8, CH	32.9, CH_2
1′	130.7, qC	132.1, qC	130.5, qC	132.7, qC	133.1, qC	130.8, qC
2′	108.5, CH	111.2, CH	108.7, CH	112.2, CH	111.3, CH	108.7, CH
3′	149.1, qC	148.5, qC	149.1, qC	150.8, qC	149.0, qC	149.1, qC
4′	149.0, qC	147.5, qC	148.6, qC	149.1, qC	149.0, qC	148.4, qC
5‘	111.1, CH	112.1, CH	111.2, CH	111.5, CH	111.9, CH	111.2, CH
6′	119.2, CH	121.0, CH	119.2, CH	120.7, CH	120.5, CH	119.0, CH
7′	55.9, CH_3	55.9, CH_3	56.0, CH_3	56.0, CH_3	55.9, CH_3	55.9, CH_3
8′	56.0, CH_3	56.0, CH_3	55.9, CH_3	56.1, CH_3	56.0, CH_3	56.0, CH_3
1″	132.5, qC	136.9, qC	136.2, qC	133.3, qC	137.4, qC	136.4, qC
2″	129.7, CH	103.7, CH	105.6, CH	103.3, CH	136.0, qC	136.9, qC
3″	114.0, CH	152.9, qC	153.3, qC	153.4, qC	127.7, CH	128.2, CH
4″	157.8, qC	137.7, qC	137.2, qC	137.7, qC	126.4, CH	125.5, CH
5″	114.0, CH	152.9, qC	153.3, qC	153.4, qC	127.7, qC	128.2, qC
6″	129.7, CH	103.7, CH	105.6, CH	103.3, CH	136.0, CH	136.9, qC
7″	55.4, CH_3	56.1, CH_3	56.2, CH_3	56.2, CH_3	21.1, CH_3	20.1, CH_3
8″		61.0, CH_3	61.0, CH_3	61.0, CH_3	21.1, CH_3	20.1, CH_3
9″		56.1, CH_3	56.2, CH_3	56.2, CH_3		

[a] In $CDCl_3$, at 100 MHz. Carbon multiplicities were determined by APT experiment. qC = quaternary, CH = methine, CH_2 = methylene, CH_3 = methyl carbons.

with a 3,4,5-trimethoxy-1-phenyl moiety. The ^{1}H and ^{13}C NMR data of **9** (Tables 4 and 5, respectively) suggested a coupling product similar to **3**. The methoxy proton singlets H_3-7″, H_3-8″, H_3-9″ (δ_H 3.81, 3.82, and 3.81, respectively) showed ^{3}J-HMBC correlations with the quaternary aromatic oxygenated carbons C-3″, C-4″, and C-5″ (δ_C 152.9, 137.7, and 152.9, respectively). The symmetric aromatic proton singlets H-2″/H-6″ (δ_H 6.62) showed ^{3}J-HMBC-correlations with the quaternary olefinic carbons C-2 (δ_C 147.3) and the aromatic oxygenated carbon C-4″. Therefore, compound **9** was determined to be 5-[3-(3,4-dimethoxyphenyl)prop-1-en-2-yl]-1,2,3-trimethoxybenzene.

Compound **10** had the same molecular formula as **9** ($C_{20}H_{24}O_5$), which indicated a coupling product with 3,4,5-trimethoxy-1-phenyl moiety. The ^{1}H and ^{13}C NMR data of **10** (Tables 4 and 5, respectively) suggested a coupling product similar to **2**, **5** and **8**. Therefore, the structure of **10** was determined to be (*E*)-5-[3-(3,4-dimethoxyphenyl)allyl]-1,2,3-trimethoxybenzene.

Compound **11** was found to have the same molecular formula as **9** and **10** ($C_{20}H_{24}O_5$), which indicated a coupling product with the 3,4,5-trimethoxy-1-phenyl moiety. The ^{1}H and ^{13}C NMR data of **11** (Tables 4 and 5, respectively) suggested a coupling product similar to **7**. Minor differences were observed in δ_H values for **11** than **10**, however, major differences were observed in δ_C values. Carbons C-2, C-2′, and C-6′ were downfield shifted as compared to those of **10** (+1.9, +3.5, and +1.5 ppm, respectively) unlike carbons C-2″/6″, which were upfield shifted (−2.3 ppm). These chemical shift differences may be attributed to the double bond position ($\Delta^{2,3}$ versus $\Delta^{1,2}$) and the effect of ring substitution. Therefore, compound **11** was determined to be (*E*)-5-[3-(3,4-dimethoxyphenyl)prop-1-enyl]-1,2,3-trimethoxybenzene.

The HRESIMS data of **14** (*m*/*z* 305.1526 for $[M+Na]^+$) suggested the molecular formula $C_{19}H_{22}O_2$, which suggested a coupling product with a xylyl moiety. The ^{1}H and ^{13}C NMR data of **14** (Tables 4 and 5, respectively) suggested a coupling product similar to **7** and **11**. The methyl singlets H_3-7″/H_3-8″ (δ_H 2.30) showed ^{3}J-HMBC correlations with the quaternary aromatic carbon C-1″ (δ_C 137.4), which was ^{3}J-HMBC correlated with H-2 (δ_H 5.77), confirming the position of the xylyl moiety. The unexpected splitting pattern in the protons H-5′, H-6′ and H-3″-H-5″, as they appeared as narrow doublets or broad singlets rather than straight doublets with regular *o*-coupling may be due a dihedral angle approaching 90° between these protons, resulting in a *J* value near zero. Therefore, the structure of **14** was determined to be (*E*)-2-[3-(3,4-dimethoxyphenyl)prop-1-enyl]-1,3-dimethylbenzene.

The HRESIMS of **15** (*m*/*z* 305.1522 for $[M+Na]^+$) suggested the same molecular formula as compound **14** and a coupling product with the xylyl moiety. Analysis of ^{1}H NMR data of **15** (Table 4) showed two overlapped *cis*-coupled olefinic protons H-1 and H-2 (δ_H 6.14, J = 5.5 and 6.13, J = 5.5, 4.4, respectively). Proton H-1 showed ^{3}J-HMBC correlations with the aliphatic methylene carbon C-3, in addition to the aromatic methane carbons C-2′, and C-6′ (δ_C 32.9, 108.7, and 119.0, respectively. Proton H-2 showed ^{3}J-HMBC correlations with the quaternary aromatic carbons C-1′ and C-1″ (δ_C 130.8 and 136.4, respectively. Therefore, compound **15** was determined to be (*Z*)-2-[3-(3,4-dimethoxyphenyl)allyl]-1,3-dimethylbenzene.

2.3. Pharmacology

Metastasis is the leading cause of cancer death. Cell migration is a prerequisite for cancer invasion and metastasis. Therefore, cell motility is suggested as a potential therapeutic target for cancer treatment.[18–21] Compounds **2–15** were evaluated for their potential use as anti-invasive agents against the metastatic breast cancer MDA-MB-231 cells using a Cultrex® Basement Membrane Extract (BME) cell invasion assay.[22–24]

Basement membranes are thin continuous sheets separating epithelial tissues from adjacent stroma (Fig. 2).[23,24] The main components of basement membranes are laminin, collagen IV, and a heparan sulfate proteoglycan.[23,24] The primary function of the basement membrane is to anchor down the epithelium to its loose connective tissue underneath. This is achieved by cell-matrix adhesions through cell adhesion molecules (CAMs).[25] The basement membrane acts as a mechanical barrier, preventing malignant cells from invading the deeper tissues.[25] Early stages of malignancy that are thus limited to the epithelial layer by the basement membrane are called carcinoma in situ.[25] Tumor invasion of basement membranes is a vital step in the complex multistage process, which leads to the formation of a metastasis.[23,24] Tumor cells cross basement membranes as they initially invade the lymphatic or blood vessels for dissemination into the circulation, and then undergo metastatic growth in the target organ. The penetration of the tumor cells into basement membranes involves steps including (i) attachment of the tumor cells to the basement membrane; (ii) Secretion of enzymes by the tumor cells leading to degradation of the adjacent basement membrane; and (iii) migration of the tumor cells into the target tissue in response to specific chemotactic stimuli.[18]

Cultrex® Basement Membrane Extract is a soluble basement membrane extract of the Engelbreth–Holm–Swarm (EHS) tumor that gels at 37 °C to form a reconstituted basement membrane. It consists of laminin I, type IV collagen, entactin, and heparan sulfate proteoglycan. Therefore, Cultrex® BME cell invasion assay provides a standardized model in vitro to quantify the degree at which invasive cells penetrate a barrier consisting of basement membrane component in response to chemoattractants and/or inhibiting compound.[23,24] It employs a simplified Boyden chamber design in which basement membrane extract form a matrigel coating on the top of a porous filter made of 8 μm polyethylene terephthalate (PET) (Fig. 2). Cells were treated with **2–15** at different concentrations 1–4 μM for 24 h, and 10% FBS was used as a chemoattractant. Compounds **2–15** inhibited the invasion of MDA-MB-231 in dose-dependent manner (Fig. 3). The anti-invasive activities for the C_6–C_3–C_6 semisynthesized methyl eugenol derivatives (Fig. 3A and C) were markedly better than the C_6–C_2–C_6 (**3**, **6**, and **9**) derivatives (Fig. 3B). The *Z* isomers represented by **4** and **15** were more active

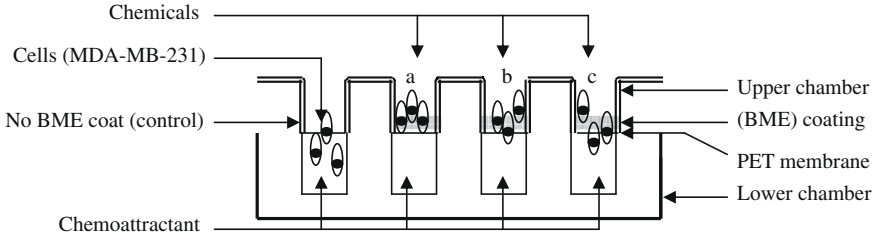

Figure 2. Schematic diagram of the cell invasion chamber used in invasion assays.

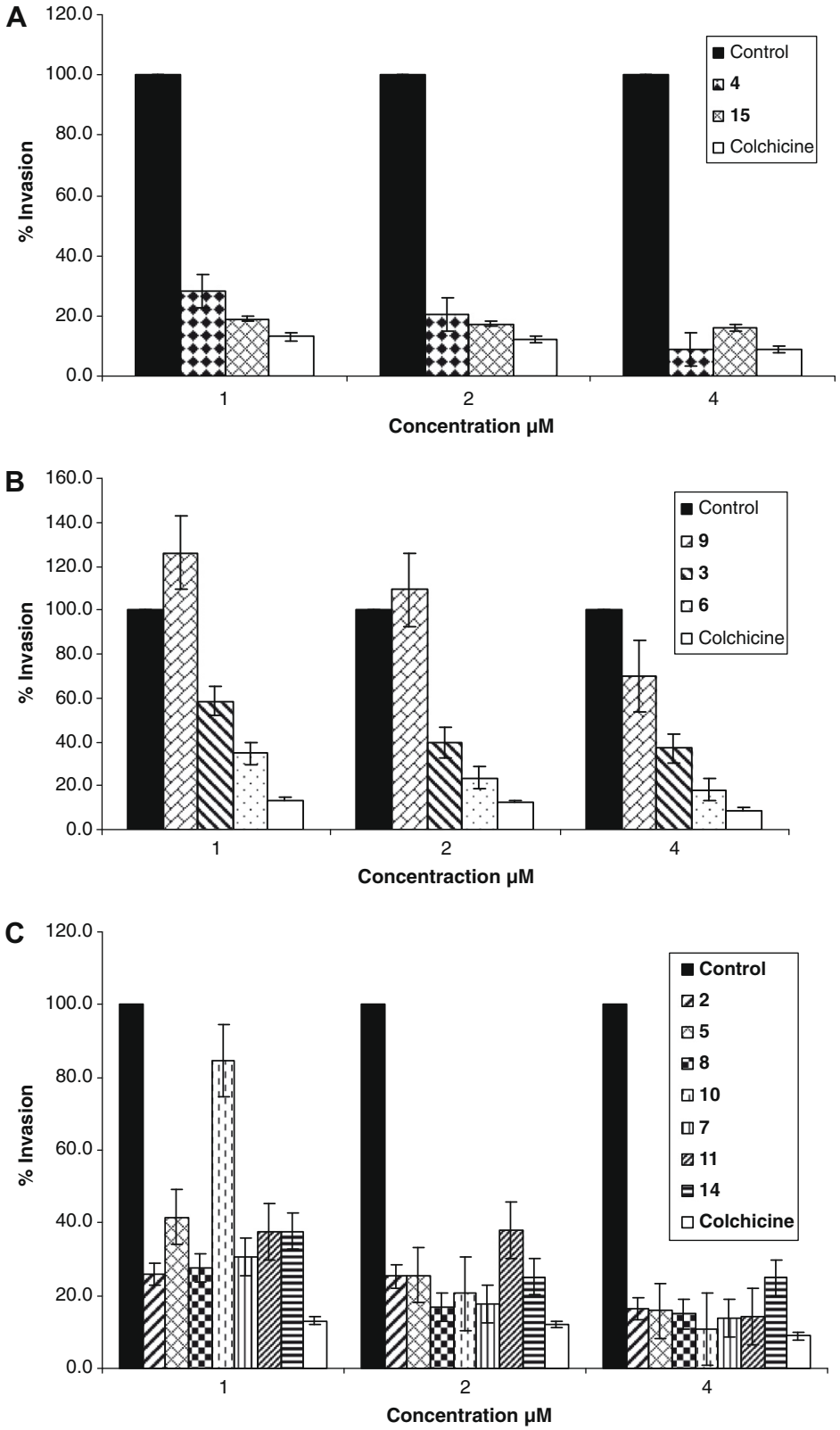

Figure 3. Anti-invasive activity of the biaryl methyl eugenol, (*Z*)-C_6–C_3–C_6, compounds **4** and **15** (A), C_6–C_2–C_6, compounds **3**, **6**, and **9** (B), and (*E*)-C_6–C_3–C_6, compounds **2**, **5**, **7**, **8**, **10**, **11**, and **14** (C) using Cultrex® 96 well BME cell invasion assay against the human metastatic breast cancer cell line MDA-MB-231.

as invasion inhibitors than the *E* isomers **2** and **14**, respectively (Fig. 3A–C). The 2″-acetoxy-containing *Z*-isomer **4** showed potent activity at 4 μM (9.0% invasion, compared to vehicle control (Fig. 3A). This activity was comparable to the activity of colchicine at the same dose level (Fig. 3A). However, the trimethoxychalcone **12** showed better activity than colchicines at 2 μM dose, data not shown (8.5% invasion vs 12.5% for colchicine). The *E*-trimethoxyphenyl and *p*-methoxyphenyl analogs **10** and **7**, respectively, also

showed potent anti-invasive activity (11.0%, 13.7% invasion, respectively) at 4 μM concentration compared to colchicine (8.9% invasion). These results were consistent with the virtual docking study (Table 1).

The cytotoxicity of compounds **2**–**15** was evaluated and compared to those of colchicine. Most methyl eugenol biaryl analogs were not cytotoxic at the 10–50 μM dose range. These results indicate that the anti-invasive activity of compounds **2**–**15** at concentration 1–4 μM is not due to a direct cytotoxic effect (Fig. 4). Cell migration through the extracellular matrix results from a continuous cycle of interdependent steps including polarization and elongation of cells.[12] Microtubule disruption is reported to provoke cytoskeleton and cell adhesion changes, which end by cell rounding.[17,23] Therefore, the methyl eugenol biaryl analogs **2**–**15** may promote their anti-invasive activity through the induction of changes in cell morphology, which alter the motility of cells in three-dimensional matrices.

Colchicine has been tested by the National Cancer Institute's Developmental Therapeutics Program (NSC757). Their results show the cytostatic effect of colchicine against the breast cancer

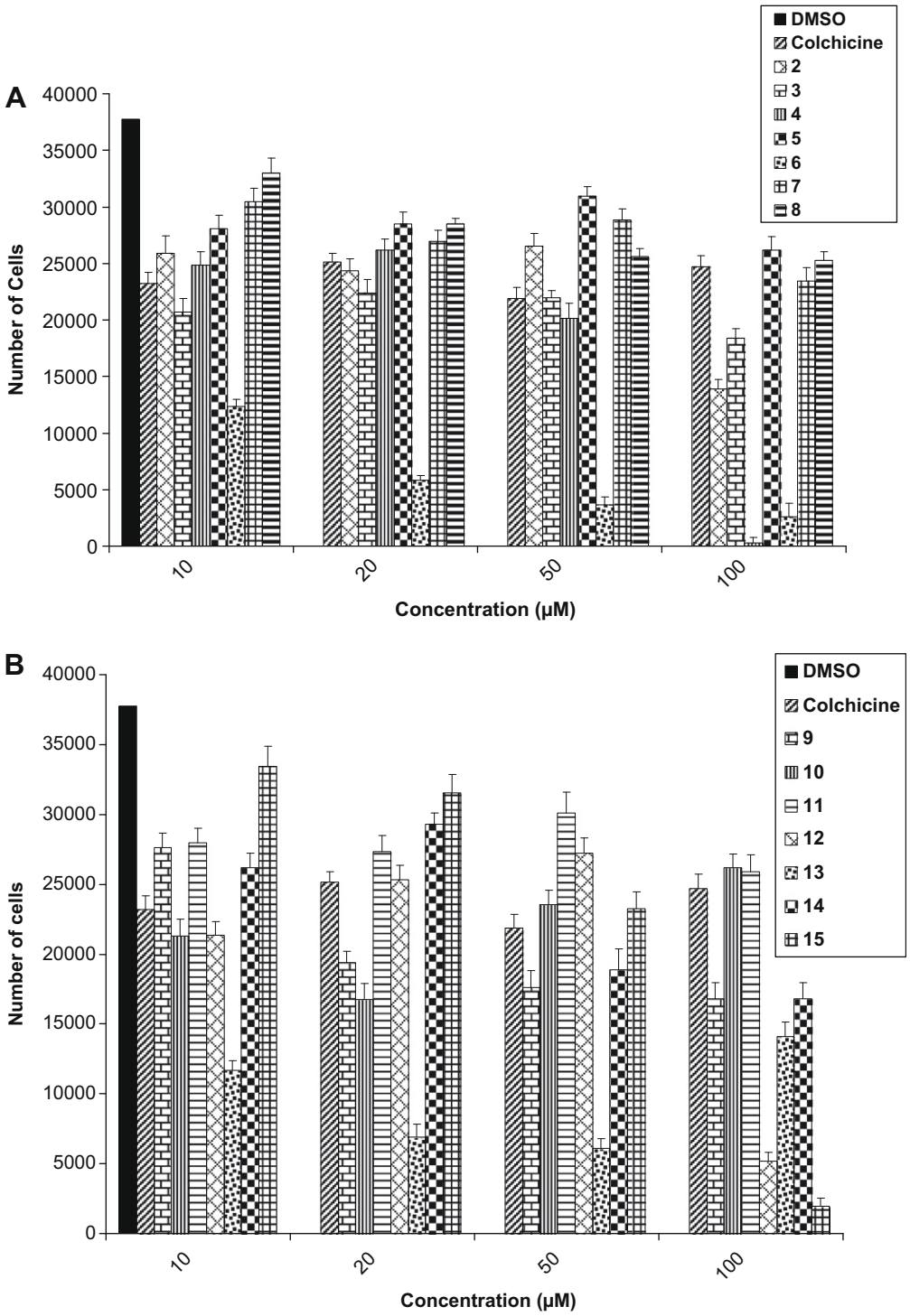

Figure 4. Cytotoxic activity of biaryl methyl eugenol derivatives **2**–**8** (A) and **9**–**15** (B) against MDA-MB-231 cells. Colchicine was used as a positive control and 10 μM DMSO at concentration as a vehicle control.

cells MCF-7 but not to MDA-MB-231.[21,26] They also established a structure–activity relationship model that describes the selective activity of colchicine toward a cell line but not to other closely related one, which was consistent with the results shown in Figure 4.[21] Therefore, the cytotoxic activities of **2**–**15** against MCF-7 cells were tested and compared with colchicine at four-dose levels (10–100 μM dose range, Fig. 5A and B). The 2-acetoxyphenyl analogs **2**–**4** showed markedly less cytotoxicity versus colchicine at a dose range of 10–50 μM (Fig. 5A). Interestingly, the trimethoxyphenyl analog **11** showed limited cytotoxicity versus the related known trimethoxychalcone **12** (Fig. 5B). This fact led to conclude that the removal of C-1 ketone of **12** did not affect the anti-invasive activity but reduced its cytotoxicity.

2.4. Pharmacophore modeling

A 3D pharmacophore mapping methodology based on distance comparison technique was built for the four most active analogs (**4**, **7**, **10**, and **12**) using DISCOtech™ module implemented in SYBYL 8.1.[27,28] DISCOtech™ is a well established module for designing pharmacophoric maps and frequently used in the process of virtual screening to discover new leads.[29,30] Given a set of molecules that are related by their ability to bind to same protein receptor, DISCOtech™ identifies features that could be elements in a pharmacophore model.[27,28] DISCOtech™ operates in distance space and can perform clique detection to generate pharmacophore hypotheses on up to 300 conformers per molecule.[27,28]

These diverse conformers are used in DISCOtech's clique detection routine to find 3D alignments of the pharmacophore features in different molecules. A clique is a subgraph in which every node is connected to every other's node. DISCOtech™ reduces the conformers to sets of pharmacophore features (nodes) and inter-feature distances (connections).[27,28]

For assignment of the pharmacophore features, a DISCOtech™ run was undertaken using **4** as the reference, 1.0 Å tolerances, and requiring models to have between three and eight matched features. DISCOtech™ produced 20 different pharmacophore models satisfying these constraints. Each of the models showed at least five matched features. Visual inspection of the resulting structural superpositions showed one model with a good structural overlay of the four compounds, while the other models did not match the biaryl system common to the four molecules.

Figure 6 shows the structural overlay corresponding to generated model. Clearly, the model has seven essential features required for high receptor binding affinity. The seven features include two hydrophobic sites, two hydrogen bond acceptor atom, and three receptor

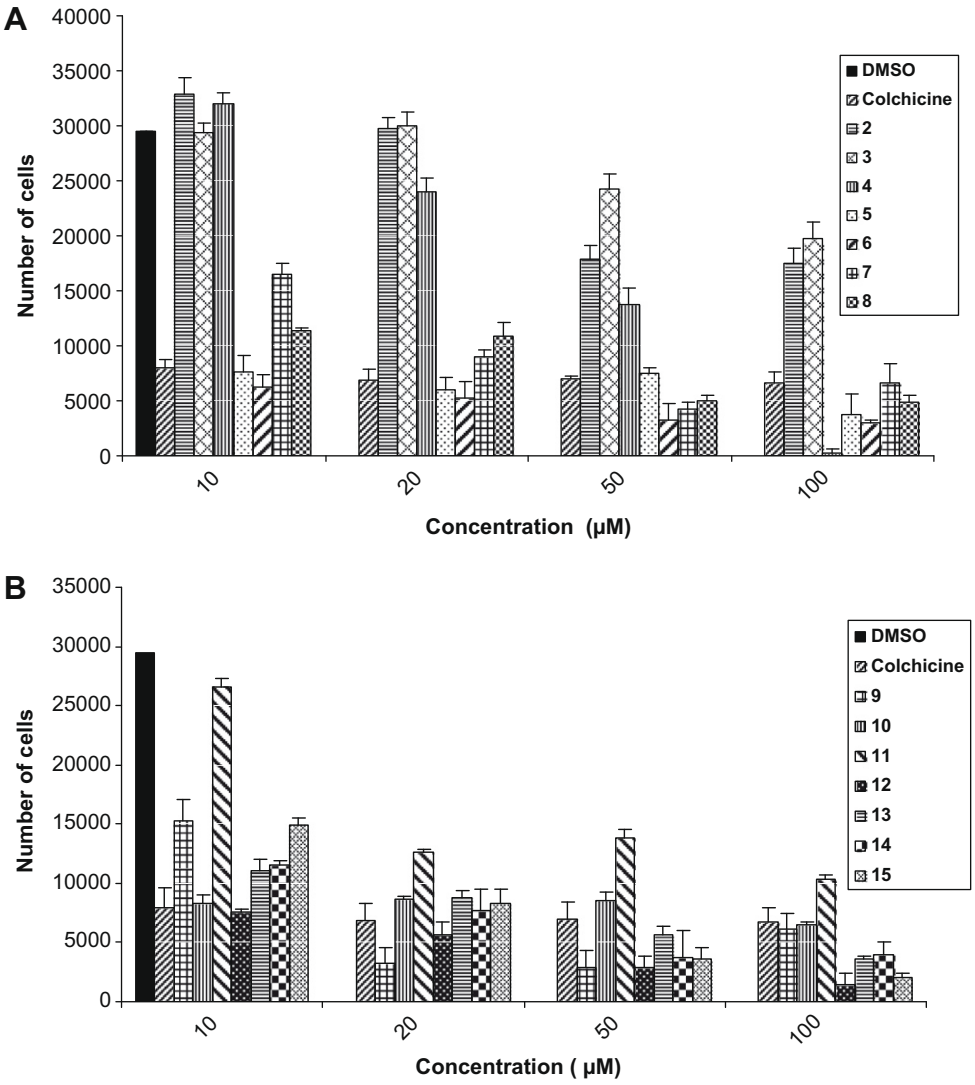

Figure 5. Cytotoxic activity of biaryl methyl eugenol derivatives **2**–**8** (A) and **9**–**15** (B) against the human breast cancer cells MCF-7. Colchicine was used as a positive control and DMSO at 10 μM concentration as a vehicle control.

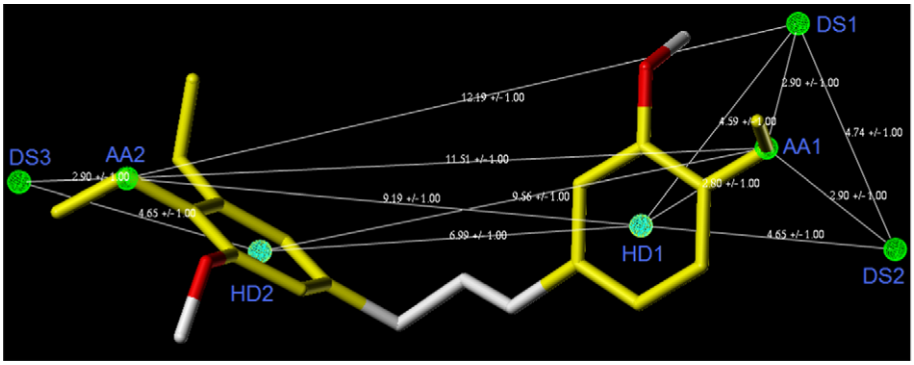

Figure 6. Pharmacophoric features and their distance relation generated by DISCOtech™ module. AA—acceptor atom, DS—donor site, HD—hydrophobic center.

donor sites. A biaryl system, di or trimethoxyphenyl moiety, and a constrained conformation features are common in all the 14 analogs and consistent with the pharmacophoric maps generated by previous colchicine site inhibitors (CSIs).[22]

The hydrophobic and the planar group serve as the rigid portion of the molecular scaffold that satisfies the overall geometric and steric requirements of binding.

Docking studies showed that the hydrophobic feature (HD1) embedded in a hydrophobic pocket consisting of the side chains of residues of side chains of Val 179 and Met 257, while the trimethoxyphenyl moiety (HD2 feature) occupies a pocket bounded by side chains of Leu 255, Ala 316, Val 318 and Ile 378. Two methoxy oxygen atoms on the HD2 ring are located within hydrogen-bond distances 2.8 and 3.4 Å to the backbone N–H groups of residues Asp (DS1) 249 and Ala 250 (DS2), respectively. AA2 features H-bonding with sulfur atom of Cys 239 (DS3) (AA2-DS3 distance of 3.2–4.2 Å). The distance between the biaryl systems is 6.99 ± 1 Å, which is in the range of the biaryl system of the different structural classes of CSIs (5.1–7.4 Å).[22] This model has the characteristic features required for an ideal pharmacophoric query, because it possessed the important interactions required for this series of CSIs and was consistent with previously reported pharmacophore models.[22]

3. Experimental section

3.1. General experimental procedures

IR spectra were recorded on a Varian 800 FT-IR spectrophotometer. The ^{1}H and ^{13}C NMR spectra were recorded in $CDCl_3$, using TMS as an internal standard, on a JEOL Eclipse NMR spectrometer operating at 400 MHz for ^{1}H and 100 MHz for ^{13}C. The HREIMS experiments were conducted at the University of Michigan on a Micromass LCT spectrometer. TLC analysis was carried out on precoated Si Gel 60 F_{254} 500 μm TLC plates, using the developing systems *n*-hexane–EtOAc (8:2) or (6:4). For column chromatography, Si Gel 60 (EMD Chemicals Inc.), 70–230 mesh, or Si Gel (Natland International Corporation), 230–400 mesh, were used. For medium pressure column chromatography (MPLC) Bakerbond octadecyl C18, 40 μm and MeOH–H_2O system were used. Photographs of cells were captured using a Nikon® Eclipse TE2000-U inverted microscope (Nikon Instruments Inc.).

3.2. Molecular modeling and docking

Three-dimensional structure building and all modeling were performed using the SYBYL Program Package, version 8.1,[31] installed on DELL desktop workstations equipped with a dual 2.0 GHz Intel® Xeon® processor running the Red Hat Enterprise Linux (version 5) operating system. Conformations of each compound were generated using Confort™ conformational analysis. Energy minimizations were performed using the Tripos force field with a distance-dependent dielectric and the Powell conjugate gradient algorithm with a convergence criterion of 0.01 kcal/(mol A).[32] Partial atomic charges were calculated using the semiempirical program MOPAC 6.0 and applying the AM1.[33]

Surflex-Dock program version 2.0 interfaced with SYBYL 8.1 was used to dock the biaryl methyl eugenol coupling derivatives to the colchicine-binding site of tubulin.[34,35] Surflex-Dock employs an idealized active site ligand (protomol) as a target to generate putative poses of molecules or molecular fragments.[36,37] These putative poses were scored using the Hammerhead scoring function.[36,37] The 3D structure (PDB 3e22) was taken from the Research Collaboratory for Structural Bioinformatics Protein Data Bank (http://www.rcsb.org/pdb).[9]

3.3. Preparation of compounds 2–4, 14, 15 by Heck reaction[14]

In a 50 mL 3-necked flask were placed equimolar quantities of methyl eugenol **1** (163.8 mg, 0.92 mM) and 2-acetoxy-iodobenzene (241.0 mg, 0.92 mM) in case of **2–4** or bromoxylene (170.3 mg, 0.92 mM) in case of **14** and **15**. Acetonitrile (14 mL), triethylamine (4 mL), palladium acetate (4.5 mg, 2 mol %) and triphenylphosphine (12.1 mg, 5 mol %) were then added and the mixtures were stirred for few minutes. Reaction flasks were then fitted to condensers and attached to a N_2 supply and a pressure relief bubbler. Each reaction mixture was stirred and heated to 85 °C for 3 h. Reactions were monitored by TLC every 1 h. At the end of reaction period, each reaction mixture was quenched by the addition of 5 g of ice. The mixtures were then extracted with EtOAc (3 × 15 mL) and the organic layers were dried over anhydrous Na_2SO_4 and concentrated under vacuum to give crude brown mixtures, which were then purified using chromatographic methods described later. Reaction of 2-iodobenzene with Ac_2O in pyridine afforded 2-acetoxyiodobenzene.

3.4. Preparation of compounds 5–13 by Suzuki coupling reaction[15]

Methyl eugenol **1** (89 mg, 0.5 mM, 1 equiv) was dissolved in DMF (2.5 mL, 0.2 M solution), and stirred at room temperature.[15] To the solution, was added 2-methoxy phenylboronic acid in case of **5** (91.2 mg, 0.6 mM, 1.2 equiv), 4-methoxy phenylboronic acid in case of **6–8** (91.2 mg, 0.6 mM, 1.2 equiv) or 3,4,5-trimethoxy phenylboronic acid in case of **9–13** (127.2 mg, 0.6 mM, 1.2 equiv) followed by addition of Na_2CO_3 (106 mg, 1.0 mM, 2 equiv) and $Pd(OAc)_2$ (11 mg, 0.05 mM, 0.1 equiv) to each reaction flask. The reaction was carried out under air atmosphere instead of O_2 and therefore 5 mol % of $Pd(OAc)_2$ was used as previously described before.[15] The reaction mixtures were heated to 50 °C, and stirred for 3 h. The mixtures were then diluted with ethyl acetate (20 mL),

and washed with aqueous NaCl solution (3 × 10 mL). The organic layers were dried over anhydrous Na_2SO_4 and filtered. The filtrates were concentrated under vacuum, and purified using chromatographic methods described below.

3.5. Chromatographic purification of 2-15

3.5.1. Acetoxyphenyl products 3 and 4

The crude brown residue obtained from Heck's reaction of **1** with 2-acetoxy-iodobenzene, was chromatographed over Si Gel 60 and eluted with (*n*-hexane–EtOAc, 8:2). The selected fraction was further subjected to MPLC using RP-C18 Si Gel (MeOH–H_2O, 6:4) to afford **2** (15 mg, 8.5%), **3** (3 mg, 38.5%), and **4** (9 mg, 23.1%).

3.5.2. Xylyl products 14 and 15

The crude product of Heck's reaction of **1** with bromoxylene was subjected to MPLC using RP-C18 Si Gel (MeOH–H_2O, gradient elution). Elution with (MeOH–H_2O, 7:3, isocratic) afforded **15** (6 mg, 23.4%) and **14**, (7.5, 29.3% mg).

3.5.3. 2-Methoxyphenyl product 5

The crude product of Suzuki coupling reaction of **1** with 2-methoxy phenylboronic acid coupling reaction was chromatographed over Si Gel column using (*n*-hexane–EtOAc, gradient elution). The selected fraction eluted with (*n*-hexane–EtOAc, 9:1) was further subjected to medium pressure column chromatography using RP-C18 Si Gel (MeOH–H_2O, 7:3, isocratic) afforded **5** (25 mg, 80%).

3.5.4. 4-Methoxyphenyl products 6–8

The crude brown product from Suzuki coupling reaction of **1** with 4-methoxy phenylboronic acid was purified using Si Gel column chromatography and (*n*-hexane–EtOAc, 9.5:0.5). The selected fractions were subjected to medium pressure column chromatography using RP-C18 Si Gel (MeOH–H_2O, 8:2, isocratic) to afford **6** (12 mg, 15%) and a mixture of two isomers. The isomers were isolated using HPLC using a Phenomenex Luna 5 μm PFP(2) 100A column, 250 × 10 mm, and MeOH–H_2O, 7:3 isocratic system to afford **7** (3 mg, 37%) and compound **8** (3.5 mg, 37%).

3.5.5. 3,4,5-Trimethoxyphenyl products 9–13

The crude brown product of Suzuki coupling reaction of **1** with 3,4,5-trimethoxy phenylboronic acid was purified over Si gel 60 (*n*-hexane–EtOAc, gradient elution). The selected fraction eluted with (*n*-hexane–EtOAc, 8:2) was subjected to MPLC using RP-C18 Si Gel (MeOH–H_2O, 5:5) to afford **9** (4.5 mg, 11%) and a mixture of two isomers. These isomers were further purified using semipreparative HPLC using a Phenomenex Luna 5 μm PFP(2) 100A column, 250 × 10 mm, and MeOH–H_2O, 7:3 isocratic system to afford **10** (3.5 mg, 25%) and **11** (2.8 mg, 25%). The fraction eluted with (*n*-hexane–EtOAc, 7:3) was purified using RP-C18 Si Gel MPLC using (MeOH–H_2O, 7:3, isocratic elution) to give the saturated chalcone **13** (10 mg, 15.1%) and the chalcone **12** (25 mg, 12.3%).

3.5.5.1. (*E*)-2-[3-(3,4-Dimethoxyphenyl)allyl]phenyl acetate (2). Colorless amorphous powder, IR ν_{max} ($CHCl_3$) 3002, 2960, 2938, 2913, 2840, 1753, 1597, 1514, 1465, 1370, 1269, 1157, 1139, 1025, 966, 916, 861 cm^{-1}; ^1H and ^{13}C NMR, see Tables 2 and 3. HRESIMS *m*/*z* 335.1265 $[M+Na]^+$ (calculated for $C_{19}H_{20}O_4$, 335.1259).

3.5.5.2. 2-[3-(3,4-Dimethoxyphenyl)prop-1-en-2-yl]phenyl acetate (3). Colorless amorphous powder, IR ν_{max} ($CHCl_3$) 3002, 2937, 2839, 1755, 1593, 1515, 1465, 1370, 1263, 1140, 1084, 1028, 914, 858 cm^{-1}; ^1H and ^{13}C NMR, see Tables 2 and 3. HRESIMS *m*/*z* 335.1250 $[M+Na]^+$ (calculated for $C_{19}H_{20}O_4$, 335.1259).

3.5.5.3. (*Z*)-2-[3-(3,4-Dimethoxyphenyl)prop-1-enyl]phenyl acetate (4). Colorless amorphous powder, IR ν_{max} ($CHCl_3$) 3002, 2960, 2938, 2912, 2839, 1761, 1682, 1595, 1514, 1514, 1465, 1371, 1269, 1139, 1026, 968, 914, 860 cm^{-1}; ^1H and ^{13}C NMR, see Tables 2 and 3. HRESIMS *m*/*z* 335.1257 $[M+Na]^+$ (calculated for $C_{19}H_{20}O_4$, 335.1259).

3.5.5.4. 1,2-Dimethoxy-4-[2-(4-methoxyphenyl)allyl]benzene (6). Colorless amorphous powder, IR ν_{max} ($CHCl_3$) 3002, 2958, 2938, 2912, 2839, 1607, 1513, 1465, 1262, 1140, 1029, 898, 837 cm^{-1}; ^1H and ^{13}C NMR, see Tables 2 and 3. HRESIMS *m*/*z* 307.1310 $[M+Na]^+$ (calculated for $C_{18}H_{20}O_3$, 307.1310).

3.5.5.5. (*E*)-1,2-Dimethoxy-4-[3-(4-methoxyphenyl)allyl]benzene (7). Colorless amorphous powder, IR ν_{max} ($CHCl_3$) 3001, 2959, 2938, 2912, 2839, 1608, 1512, 1465, 1268, 1155, 1139, 1027, 967, 836 cm^{-1}; ^1H and ^{13}C NMR, see Tables 4 and 5. HRESIMS *m*/*z* 307.1313 $[M+Na]^+$ (calculated for $C_{18}H_{20}O_3$, 307.1310).

3.5.5.6. (*E*)-1,2-Dimethoxy-4-[3-(4-methoxyphenyl)prop-1-enyl]-benzene (8). Colorless amorphous powder, IR ν_{max} ($CHCl_3$) 3001, 2958, 2938, 2913, 2839, 1608, 1513, 1465, 1267, 1139, 1026, 966, 860, 834 cm^{-1}; ^1H and ^{13}C NMR, see Tables 4 and 5. HRESIMS *m*/*z* 307.1313 $[M+Na]^+$ (calculated for $C_{18}H_{20}O_3$, 307.1310).

3.5.5.7. 5-[3-(3,4-Dimethoxyphenyl)prop-1-en-2-yl]-1,2,3-trimethoxybenzene (9). Colorless amorphous powder, IR ν_{max} ($CHCl_3$) 3001, 2939, 2839, 1586, 1511, 1464, 1412, 1338, 1266, 1131, 1027, 1002 cm^{-1}; ^1H and ^{13}C NMR, see Tables 4 and 5. HRESIMS *m*/*z* 367.1509 $[M+Na]^+$ (calculated for $C_{20}H_{24}O_5$, 367.1521).

3.5.5.8. (*E*)-5-[3-(3,4-Dimethoxyphenyl)allyl]-1,2,3-trimethoxybenzene (10). Colorless amorphous powder, IR ν_{max} ($CHCl_3$) 3000, 2960, 2940, 2911, 2840, 1592, 1510, 1464, 1331, 1267, 1130, 1026, 1002, 966 cm^{-1}; ^1H and ^{13}C NMR, see Tables 4 and 5. HRESIMS *m*/*z* 367.1519 $[M+Na]^+$ (calculated for $C_{20}H_{24}O_5$, 367.1521).

3.5.5.9. (*E*)-5-[3-(3,4-Dimethoxyphenyl)prop-1-enyl]-1,2,3-trimethoxybenzene (11). Colorless amorphous powder, IR ν_{max} ($CHCl_3$) 3001, 2960, 2940, 2913, 2840, 1592, 1514, 1465, 1330, 1266, 1130, 1027, 1001, 965 cm^{-1}; ^1H and ^{13}C NMR, see Tables 4 and 5. HRESIMS *m*/*z* 367.1518 $[M+Na]^+$ (calculated for $C_{20}H_{24}O_5$, 367.1521).

3.5.5.10. (*E*)-2-[3-(3,4-Dimethoxyphenyl)prop-1-enyl]-1,3-dimethylbenzene (14). Colorless amorphous powder, IR ν_{max} ($CHCl_3$) 3003, 2937, 2839, 1592, 1515, 1465, 1264, 1153, 1139, 1028, 976, 857 cm^{-1}; ^1H and ^{13}C NMR, see Tables 4 and 5. HRESIMS *m*/*z* 305.1526 $[M+Na]^+$ (calculated for $C_{19}H_{22}O_2$, 305.1517).

3.5.5.11. (*Z*)-2-[3-(3,4-Dimethoxyphenyl)allyl]-1,3-dimethylbenzene (15). Colorless amorphous powder, IR ν_{max} ($CHCl_3$) 3002, 2958, 2939, 2913, 2839, 1585, 1512, 1466, 1267, 1139, 1026, 965, 858 cm^{-1}; ^1H and ^{13}C NMR, see Tables 4 and 5. HRESIMS *m*/*z* 305.1522 $[M+Na]^+$ (calculated for $C_{19}H_{22}O_2$, 305.1517).

3.6. Invasion assay

Invasion activities of the methyl eugenol derivatives were measured using Trevigen's Cultrex® 96 well Basement Membrane Extract (BME) cell invasion assay kit against the highly metastatic human breast cancer cell line MDA-MB-231.[23,24] This assay employs a simplified Boyden Chamber design with an 8 μm polyethylene terephthalate (PET) membrane. Detection of cell invasion is quantified using calcein-AM. The cells internalize calcein-AM, and intracellular esterases cleave the acetomethylester (AM) moiety to generate

free calcein, which fluoresces brightly, and this fluorescence used to quantify the number of cells that have invaded across BME. The bottom plate was read at 485 nm excitation, and 520 nm emission using BioTeck® microplate reader to obtain relative fluorescence unit (RFU). The RFU values were converted into cell number using a standard curve. The % invasion was obtained by dividing the number of cells that invaded (through the BME) by the number of cells that migrated (no coating).[23,24]

3.7. MTT assay

About 100 μL containing 15,000 cells/well (MDA-MB-231) or 12,000 cell/well (MCF-7) cell suspensions were added into 96-well microtiter plates. Inoculates were pre-incubated for 24 h at 37 °C and 5% CO_2 for stabilization.[21,26] Tested compound doses were examined in triplicates. Cells were then treated with tested compounds and incubated for 72 h at 37 °C, in a 5% CO_2 atmosphere at 85% humidity. Each well was treated with 20 μL MTT solution (2.5 mg/mL) and incubated for 4 h. Formazan produced was then dissolved by the addition of 100 μL /well of Detergent Reagent, Trevogen® (in case of MDA-MB-231) or isopropanol (in case of MCF-7) followed by overnight incubation at rt in dark. The optical density (OD) was measured at 570 nm using a BioTeck® Synergy 2 microplate reader against a blank prepared from cell-free cultures. The number of cells/well was calculated using the calibration curve equation.[21,26]

3.8. Pharmacophore generation

The four most active analogs, **4**, **7**, **10**, and **12**, were used to build the pharmacophoric map using DISCOtech™ module.[22,28,29] The structures of these compounds were constructed manually using SYBYL 8.1, minimized using the Tripos force field to obtain a local minimum, and partial atomic charges were calculated using the semiempirical program MOPAC 6.0 and applying the AM1.[28,29] Diverse conformers were generated for each structure using the Confort™ conformational analysis tool in SYBYL. Pharmacophore model was derived using DISCOtech™.[22,28–30] Assignment of the initial pharmacophore features for the DISCO based pharmacophore mapping was done using the following features—aromatic and aliphatic ring centroids as hydrophobic centers, hydrogen bond donors and acceptors, and external site points representing receptor-associated hydrogen bond acceptor sites and donor sites.

Acknowledgment

The Egyptian Government is acknowledged for the fellowship support to F.M.A.B.

Supplementary data

Supplementary data (^{1}H and ^{13}C NMR spectra of compounds **2–11** and **14**–**15** and HPLC chromatogram of isolations of compound **7**, **8**, **10**, and **11**) associated with this article can be found, in the online version, at doi:10.1016/j.bmc.2009.12.019.

References and notes

1. Butler, M. S. *Nat. Prod. Rep.* **2008**, *25*, 475.
2. Tozer, G. M.; Kanthou, C.; Parkins, C. S.; Hill, S. A. *Int. J. Exp. Pathol.* **2002**, *83*, 21.
3. Ducki, S.; Mackenzie, G.; Lawrence, N. J.; Snyder, J. P. *Journal Med. Chem.* **2005**, *48*, 457.
4. Siemann, D. W.; Chaplin, D. J.; Walicke, P. A. *Expert Opin. Invest. Drugs* **2009**, *18*, 189.
5. Belletti, B.; Nicoloso, M. S.; Schiappacassi, M.; Berton, S.; Lovat, F.; Wolf, K.; Canzonieri, V.; D'Andrea, S.; Zucchetto, A.; Friedl, P.; Colombatti, A.; Baldassarre, G. *Mol. Biol. Cell* **2008**, *19*, 2003.
6. Kingston, D. G. I. *Journal Nat. Prod.* **2009**, *72*, 507.
7. Hadfield, J. A.; Ducki, S.; Hirst, N.; McGown, TA. T. *Prog. Cell Cycle Res.* **2003**, *5*, 309.
8. Farag, R. S.; Shalaby, A. S.; El-Baroty, G. A.; Ibrahim, N. A.; Ali, M. A.; Hassan, E. M. *Phytoth. Res.* **2004**, *18*, 30.
9. Cormier, A.; Marchand, M.; Ravelli, R. B.; Knossow, M.; Gigant, B. *EMBO Rep.* **2008**, *9*, 1101.
10. Ravelli, R. B.; Gigant, B.; Curmi, P. A.; Jourdain, I.; Lachkar, S.; Sobel, A.; Knossow, M. *Nature* **2004**, *428*, 198.
11. Uppuluri, S.; Knipling, L.; Sackett, D. L.; Wolfft, J. *Proc. Natl. Acad. Sci.* **1993**, *90*, 11598.
12. Tripathi, A.; Fornabaio, M.; Kellogg, G. E.; Gupton, J. T.; Gewirtz, D. A.; Yeudall, W. A.; Vega, N. E.; Mooberry, S. L. *Bioorg. Med. Chem.* **2008**, *16*, 2235.
13. Spinner, E. *Journal Chem. Soc.* **1956**, 1590.
14. Bianco, A.; Cavarischia, C.; Guiso, M. *Nat. Prod. Res.* **2006**, *20*, 93.
15. Jung, Y. C.; Mishra, R. k.; Yoon, C. H.; Jung, K. W. *Org. Lett.* **2003**, *5*, 2231.
16. Oluwadiya, J. O.; Whalley, W. B. *Journal Chem. Soc., Perkin Trans. 1* **1978**, 88.
17. David, G. C.; Jason, E. F.; Coffey, R. S.; Johnson, H. E. *J. Am. Chem. Soc.* **1958**, *80*, 5756.
18. Albini, A.; Iwamoto, Y.; Kleinman, H. K.; Martin, G. R.; Aaronson, S. A.; Kozlowski, J. M.; McEwan, R. N. *Cancer Res.* **1987**, *47*, 3239.
19. Friedl, P.; Wolf, K. *Nat. Rev.* **2003**, *3*, 362.
20. Deschesnes, R. G.; Patenaude, A.; Rousseau, J. L. C.; Fortin, J. S.; Ricard, C.; Côté, M. F.; Huot, J.; Gaudreault, R. C.; Petitclerc, E. *JPET* **2007**, *320*, 853.
21. Cunningham, A. R.; Cunningham, S. L.; Day, B. W. *Bioorg. Med. Chem.* **2003**, *11*, 5249.
22. Nguyen, T. L.; McGrath, C.; Hermone, A. R.; Burnett, J. C.; Zaharevitz, D. W.; Day, B. W.; Wipf, P.; Hamel, E.; Gussio, R. A. *Journal Med. Chem.* **2005**, *48*, 6107.
23. Tamilarasan, K. P.; Kolluru, G. K.; Rajaram, M.; Indhumathy, M.; Saranya, R.; Chatterjee, S. *BMC Cell Biol.* **2006**, *7*, 17.
24. Borghesani, P. R.; Peyrin, J. M.; Klein, R.; Rubin, J.; Carter, A. R.; Schwartz, P. M.; Luster, A.; Corfas, G.; Segal, R. A. *Development* **2002**, *6*, 1435.
25. Liotta, L. A.; Tryggvason, K.; Garbisa, S.; Ian Hart; Foltz, C. M.; Shafie, S. *Nature* **1980**, *284*, 67.
26. Hajduch, M.; Mihal, V.; Minarik, J.; Faber, E.; Safarova, M.; Weigl, E.; Antalek, P. *Cytotechnology* **1996**, *19*, 243.
27. Martin, Y. C.; Bures, M. G.; Danaher, E. A.; DeLazzer, J.; Lico, I.; Pavlik, P. A. *Journal Comput. Aided Mol. Des.* **1993**, *7*, 83.
28. Clark, R. D. *Journal Chem. Inf. Comput. Sci.* **1997**, *37*, 1181.
29. Marriott, D. P.; Dougall, I. G.; Meghani, P.; Liu, Y-J.; Flower, D. R. *Journal Med. Chem.* **1999**, *42*, 3210.
30. Spadoni, G.; Balsamini, C.; Diamantini, G.; Di Giacomo, B.; Tarzia, G.; Mor, M.; Plazzi, P. V.; Rivara, S.; Lucini, V.; Nonno, R.; Pannacci, M.; Fraschini, F.; Stankov, B. M. *Journal Med. Chem.* **1997**, *40*, 1990.
31. Tripos Associates. SYBYL *Molecular Modeling Software*, version 8.0; Tripos Associates: St. Louis, MO, **2007**; http://www.tripos.com.
32. Clark, M.; Cramer, R. D., III; van Opdenbosch, N. *Comput. Chem.* **1989**, *10*, 982.
33. Stewart, J. J. *Journal Comput. Aided Mol. Des.* **1990**, *4*, 1.
34. Kellenberger, E.; Rodrigo, J.; Muller, P.; Rognan, D. *Proteins* **2004**, *57*, 225.
35. Jain, A. N. *Journal Med. Chem.* **2003**, *46*, 499.
36. Welch, W.; Ruppert, J.; Jain, A. N. *Chem. Biol.* **1996**, *3*, 449.
37. Ruppert, J.; Welch, W.; Jain, A. N. *Protein Sci.* **1997**, *6*, 524.